NANO LETTERS
Letter
pubs.acs.org/NanoLett

Tracking Nanoparticle Diffusion and Interaction during Self-Assembly in a Liquid Cell

Alexander S. Powers,[†] Hong-Gang Liao,[§] Shilpa N. Raja,[‡,§] Noah D. Bronstein,[†] A. Paul Alivisatos,[†,§,∥] and Haimei Zheng*[,‡,§]

[†]Department of Chemistry and [‡]Department of Materials Science and Engineering, University of California, Berkeley, California 94720, United States

[§]Materials Sciences Division, Lawrence Berkeley National Laboratory, Berkeley, California 94720, United States

[∥]Kavli Energy NanoScience Institute, Berkeley, California 94720, United States

Supporting Information

ABSTRACT: Nanoparticle self-assembly has been well studied theoretically, but it remains challenging to directly observe and quantify individual nanoparticle interactions. With our custom image analysis method, we track the trajectories of nanoparticle movement with high precision from a stack of relatively noisy images obtained using liquid cell transmission electron microscopy. In a time frame of minutes, Pt−Fe nanoparticles self-assembled into a loosely packed hcp lattice. The energetics and stability of the dynamic assembly were studied quantitatively. From velocity and diffusion measurements, we experimentally determined the magnitude of forces between single particles and the related physical properties. The results illustrate that long-range anisotropic forces drive the formation of chains, which then clump and fold to maximize close range van der Waals interactions.

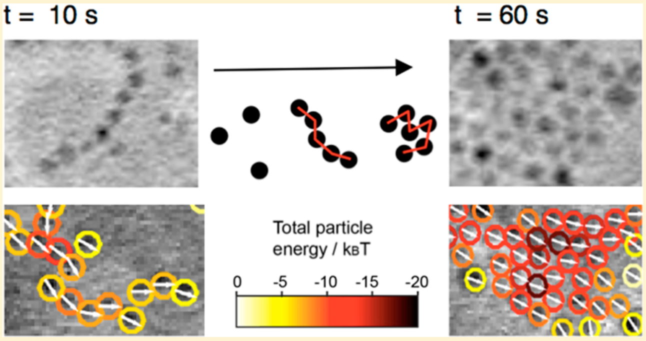

KEYWORDS: *Nanocrystals, self-assembly, Pt−Fe nanoparticles, particle tracking, image analysis, liquid cell TEM*

The unique optical and electronic properties of nanoparticles are promising for applications in batteries,[1,2] solar cells,[3−5] recording media,[6,7] catalysts,[8,9] electronic components,[10,11] and others.[12] However, nanoparticles organized into controlled patterns are necessary for many device applications, stimulating intense study of nanoparticle self-assembly.[1−11] Self-assembly on the nanoscale is also an important process for biological systems, such as microtubules, viral capsids, and amyloid fibers.[13−16] To manipulate self-assembly requires understanding the underlying driving forces and creating general models that apply over a variety of material systems.[17−19]

Assembled nanomaterials take on forms of varying dimensionality including linear chains and loops (1D), compact sheets (2D), and 3D crystals. Assembly of one-dimensional (1D) chains is a theme that emerges across diverse experiments with different materials and conditions.[20−29] Chains are evidence of basic anisotropy in the interactions between nanoparticles leading to oriented attachment and chain growth. However, the similarity in assembly appearance fails to capture a range of distinct driving forces. For example, magnetic nanoparticles with relatively strong, long-range magnetic forces align their dipoles into rigid chains[29] while semiconductor nanocrystals possess electric dipoles due to an uneven distribution of charges from crystal faceting.[31,32] Additionally, even in neutral metallic particles like Au and Pt, an anisotropic distribution of capping agents on nanoparticle surfaces leads to preferred interaction of the uncapped region.[26−28] These forces differ in range and strength altering the kinetics and patterns of assemblies. Isotropic forces that operate at close range also play a critical role in holding nearby particles together; these include van der Waal forces, ligand interactions, and bonding between bare nanoparticle surfaces.[23,30,33] The Pt−Fe nanoparticles used in this study are in a disordered chemical phase leading to superparamagnetism which would normally accompany a lack of static dipole to drive assembly in the absence of external fields.[34] However, magnetic forces could still be at play; previous studies show that superparamagnetic particles can still assemble rapidly as their thermally fluctuating dipoles are stabilized by interactions with many neighbors.[35] Because the nonbulk electric or magnetic properties are often not known and the particles have complex anisotropic structure, the combination of these forces is complicated to predict a priori.

In this study, we use liquid cell transmission electron microscopy (TEM) to track nanoparticles and directly measure nanoparticle interactions, which offers a quantitative and data

Received: July 18, 2016
Revised: October 6, 2016
Published: November 9, 2016

DOI: 10.1021/acs.nanolett.6b02972
Nano Lett. 2017, 17, 15−20

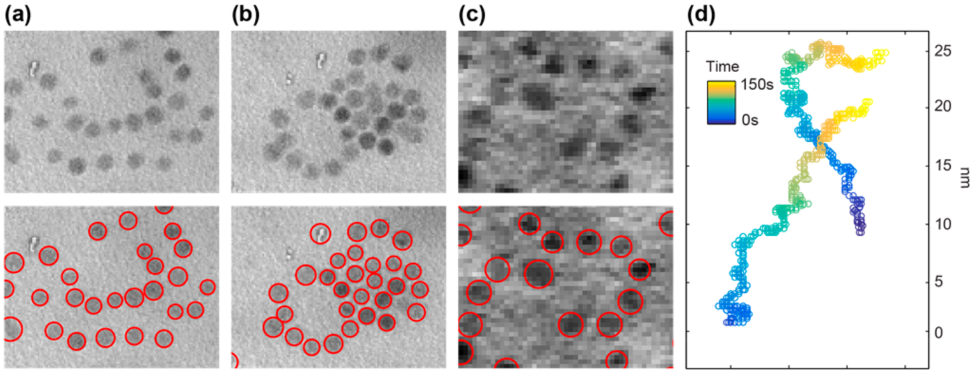

Figure 1. Observation and tracking of nanoparticle assembly in a liquid cell. (a) Automatic detection of $PtFe_3$ nanoparticles during the assembly process. (b) Detection of particles in a packed assembly. (c) Detecting particles in a low-resolution image with noisy background. (d) Successful tracking of two nearby (potentially interacting) diffusing particles over the course of 150 s or 750 frames.

driven description of assembly in comparison to previous observational studies or computational simulations. In the liquid cell, nanoparticles become adsorbed to a transparent window while retaining 2D movement akin to surface diffusion. With a reduced velocity, interparticle interactions become significant leading to assembly.[24] Previous studies using liquid TEM to study nanoparticle assembly are limited to qualitative observations or relatively simple assemblies like chains.[24,36−39] Employing computational methods, we analyze the dynamics of not only many isolated particles but intermediate clusters and relative particle velocities as assembly progresses. This approach elucidates how chains of nanoparticles form and ultimately pack into denser configurations. We also demonstrate a new approach to calculate the magnitude of net interparticle forces from velocity trajectories and diffusion behavior, properties that are otherwise not currently attainable on a single particle level. With these interaction potentials defined, the contributions of different driving forces to the stabilizing energy can be calculated. Computational simulations of assembly would benefit from these parameters. Simulation data could be corroborated with precise experimental data and particle forces provide a starting point for simulating nanoparticle interactions in diverse environments.

Liquid cells were fabricated using previously published procedures described briefly.[37] Electron transparent silicon nitride windows with a thickness of 13 nm were deposited on silicon wafers followed by lithographic patterning and etching. An indium thin film spacer created a 100−120 nm thick cavity between two parallel windows. Pt(acetylacetonate)$_2$ (20 mg/mL) and Fe(acetylacetonate)$_2$ (20 mg/mL) were dissolved in pentadecane, oleylamine, and oleic acid (5:4:1 vol/vol/vol). Thirty picoliters of growth solution was injected into the liquid cell and drawn into the viewing cavity by capillary action. The cell was sealed with epoxy and placed into the microscope as a standard sample. The $PtFe_3$ nanoparticles were grown in situ by exposure of growth solution to the electron beam.[36] Particles were crystalline and grew slowly by monomer attachment and occasional coalescence of small particles. The spherical particles were on average 3−4 nm in diameter with a standard deviation of 10−15% (see Supporting Information for further discussion of size and morphology). A JEOL 3010 TEM operated at 300 kV and a FEI monochromated F20 UT Tecnai microscope operated at 200 kV were used for imaging. A beam current density of 1×10^5 to 8×10^5 A/m^2 was maintained for the study. A CM200 microscope TEM with an energy-dispersive X-ray spectroscopy (EDS) detector was used for elemental analysis of the nanoparticles in the liquid cell.

All the movies have a frame rate of 5 frames per second. Movie S1 covers an imaging area of 500 nm × 500 nm with a resolution of 0.9 nm/pixel. The intent here was for rigorous statistical analysis of the roughly 1000 nanoparticles visible. Movie S2 has a higher resolution at 0.2 nm per pixel covering an area of 100 × 100 nm affording detailed measurements of nanoparticle trajectories.

A custom image analysis algorithm in Matlab enables quantitative study of assembly and allows for new types of analysis to be applied. A particle detection and tracking algorithm was developed specifically for noisy and low contrast TEM images containing nanoparticles with a large distribution of sizes and imperfect shapes (Figure 1). The detection step isolates objects at different length scales enabling a threshold function that depends on size and can be adapted to the scale of high- and low-frequency noise in the image (more details are available in Supporting Information). The advantages of this approach are to capture particles at multiple size scales, avoid any preprocessing of background intensity fluctuations (which occur often over the hundreds of frames in a liquid cell video), and distinguish overlapping particles. The particle identification accuracy in a noisy environment is 95% (Figure 1e), while the accuracy for typical images is 97%. Tracking of the particles was completed with another custom algorithm that accounts for gaps in detection where particles might become obscured by low contrast or bubbles in the liquid film (Figure 1d).

Transformation from a disordered, low-density arrangement of particles to a 2D loosely packed lattice of particles with areas of close packing was observed over the course of 1 min (Figure 2a, also see Movie S1). Before forming a 2D lattice, the particles align into well-defined 1D chains that suggest a hierarchical mechanism for assembly that proceeds through this intermediate form. In order to describe this transformation more precisely, the particles in each frame are classified into three different configurations: chains, close-packed, and unconnected (representative examples in Figure 2b). This procedure is performed algorithmically looking at 800 particles based on the identified particle locations. Specifically, particles with greater than four neighbors are classified as packed (along with these neighbors). Using the remaining particles, chains are then defined based on particle proximity as well as a limit on the curvature of the chain. The minimum chain size is three particles. The remaining particles are then classified as unconnected.

DOI: 10.1021/acs.nanolett.6b02972
Nano Lett. 2017, 17, 15−20

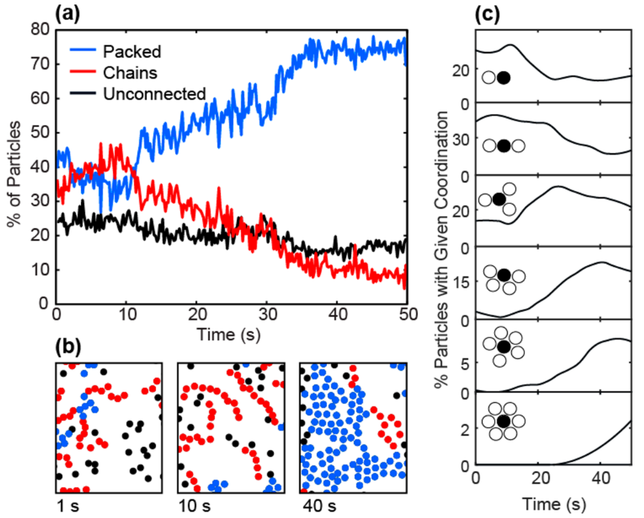

Figure 2. Configurations of nanoparticles during assembly. (a) Distribution of particles classified into three different configurations over the course of the assembly process. (b) Particles locations color-coded to correspond to configurations in panel a. These are representative details rather than the entire observation image. (c) Distribution of particles with different numbers of surrounding neighbors from 1−6 neighbors.

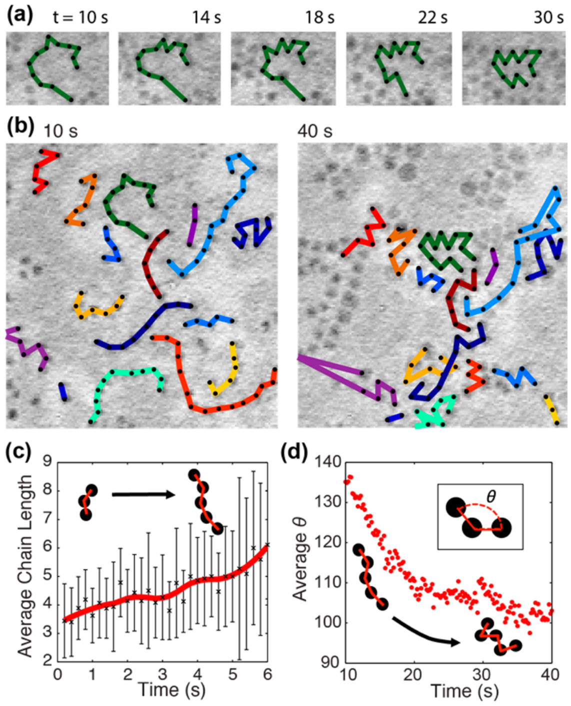

Figure 3. Dynamics of nanoparticles aligned in one-dimensional chains. (a) Chains formed at the beginning of assembly have a particle connectivity that is tracked over time to illustrate folding and clumping behavior. (b) Clumped chains combine and fold to form packed structures (c) Chain growth leads to increase in average chain length and broadening of length distribution. (d) The angle θ is defined by three adjacent particles in a chain. Maintaining the same chain connectivity over time, the average θ is measured over all particles in all chains.

Applying this analysis over the course of the video (Movie S1), the initial distribution of nearly equal chains and packed particles shifts to 75% packed and 10% chains within 1 min (Figure 2a). As the percent of particles in the packed configuration increases, the percent in chains decreases at a similar rate. Thus, the packed particles are not being formed by the addition of unconnected nanoparticles subunits but directly from the already semiordered particles in chains. At 40 s, the particles reach an equilibrium with the majority in the packed form; the distribution stops shifting with only small remaining fluctuations.

This assembly behavior indicates that the packed phase is not growing at a defined interface in the manner of a crystalline solids[40,41] but bears a resemblance to hierarchical descriptions of protein self-assembly.[13,14] However, typical spherical nanoparticles are loosely analogous to the hard sphere-packing model used to illustrate the atomic structure of solid crystals. Along these lines and to better elucidate the ordering of the particles, we track the distribution of particles with different numbers of neighbors (Figure 2c). Only a few particles become hexagonally close-packed having the optimal coordination number of six for uniform hard spheres. Even after many of the particles achieve a coordination number of three it takes more time for particles to obtain four or five neighbors. We propose that chains provide an initial means of loosely associating nanoparticles, but further limited motion leads the particles to settle into successively more ideal coordination environments. However, because the individual nanoparticle motion becomes limited by association with neighbors, vacancies likewise become trapped leading to further nonideal coordination.

In order to demonstrate the role of chain intermediates in self-assembly, we investigate chain growth and dynamics. During the first 10 s, chains grow longer by attachment of nanoparticle subunits to the chain ends leading the average chain length to increase from three to six particles (Figure 3c). Initially, the chains are similar in length but the distribution broadens significantly (with some greater than 10 particles, see Figure 3b) leading to an increase in length standard deviation (Figure 3c).

The same groups and connections between particles defining the chains at 10 s are then tracked for the duration of the video (Figure 3a,b). Particles largely stay associated with their neighbors from the original chain moving as a group into their final positions in the loosely packed configuration. A few chains split apart into subgroups. The chains either fold to form locally packed clumps or they associate side by side. In order to measure the average chain behavior, we measure the angle formed by any three adjacent particles in a chain (Figure 3d). Averaging over all the chains, the angle between particles decreases significantly indicating this folding behavior was characteristic and occurred gradually. Chain folding explains the trends in coordination behavior of forming three coordinate particles before four, five, or six. Higher coordination occurs upon further clumping or multiple clumps drifting together.

To study the nanoparticle forces responsible for the observed dynamics, we track the motion of pairs of nanoparticles and their velocity upon being brought into close range. The particles are bound to the two silicon nitride windows, likely through strong electrostatic interactions, and consequently confined to slowed 2D motion.[24] The diffusivity for several isolated particles was measured to be $D = 0.11 \pm 0.08$ nm^2/s (Figure S11), which was comparable to previously reported values in liquid cells but is orders of magnitude slower than the predicted value in liquid $D = (k_B T/6\pi\mu r) = 1.74 \times 10^7$ nm^2/s where μ is the viscosity of oleylamine.[24] We found that the diffusivity depended strongly on particle size with smaller particles diffusing significantly faster (Figure 4a). However, the relationship did not follow the expected $1/r$ trend, possibly due to the interaction with the window depending on the surface area of particle facets.

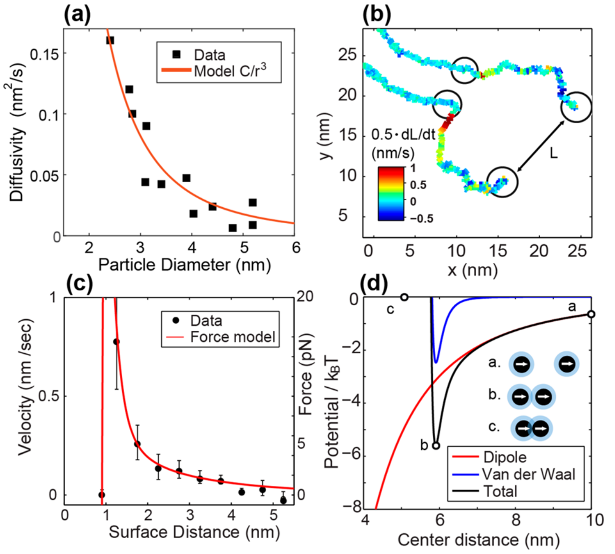

Figure 4. Interactions and forces between individual nanoparticles. (a) The diffusion coefficient was measured for particles of various sizes by calculating the mean squared displacement vs time (see Figure S11). (b) Colored lines indicate the tracked paths of two nearby nanoparticles. The estimated relative particle velocity is used to color code the paths. (c) Averaged data for relative velocity versus surface-to-surface distance between particles (black). The fitted line (red) indicates the equation of proposed interparticle forces. (d) Proposed potential energy relative to thermal energy of two 5 nm nanoparticles approaching each other with aligned dipoles. Cartoon representation of inorganic cores (black) and ligand shells (blue) at different points along potential curve.

Because the particles are subject to diffusive and camera drift motion, we track the length of the surface-to-surface distance between pairs of particles, L, to obtain a relative individual velocity as $0.5(\mathrm{d}L/\mathrm{d}t)$ (Figure 4b). This distance fluctuates randomly until it reaches approximately 6 nm from surface-to-surface whereupon the particles are strongly attracted to each other. The range of interaction is extended and stronger if a single particle nears a cluster or chain of adjacent particles as their individual forces act in concert. At a surface-to-surface distance of 1.09 ± 0.36 nm (Figure S18), nanoparticle motion halts due to steric repulsion by the ligand shells, but the motion is slowed starting at a 2 nm separation. Literature values for the thickness of oleylamine and oleic acid shells range from 1 to 2 nm in liquid, suggesting in this study that the ligands are not tightly packed on the NP surface such that they can interpenetrate to some extent.[42−44]

The velocity versus distance data relates to the functional form of the forces exerted by a single nanoparticle. The velocity of a diffusing spherical particle in a viscous medium can be related to the applied force directly through the drag coefficient derived with the Stokes−Einstein equation and the diffusion coefficient (Figure 4c and Supporting Information for calculation). We then propose the interaction potential energy equation for two particles

$$U(l, R_i, R_j) = \frac{\lambda}{|l|^3}[3(\hat{m}_i\cdot\hat{l})(\hat{m}_j\cdot\hat{l}) - \hat{m}_i\cdot\hat{m}_j] - \frac{\beta}{(l - R_i - R_j)^6} + \frac{\alpha}{(l - R_i - R_j)^{12}}$$

where $\lambda = m_i m_j \mu_0/4\pi$ with m as the particle's net magnetic dipole moment, l is the distance between the particle centers, $\hat{m}$ is the unit vector of the particle dipole, R is the radius of a particle, and β and α are unknown coefficients. Assuming aligned dipoles, the derivative of this potential fit closely to the force versus distance data (Figure 4c). It is noted that we study the interaction of relatively isolated but similarly sized pairs of particles. The potential combines both a dipole interaction term with a close range isotropic interaction modeled as a Lennard-Jones potential. The latter term is due to attractive van der Waals forces between spherical particles and interactions between ligand shells, depending only on the surface-to-surface distance. More complex potentials exist for colloidal particles describing exactly the van der Waals attraction (dependent on the material's Hamaker constant) and surfactant repulsion (dependent on the number of ligands, thickness of ligand shell, and solvent properties). However, previous simulation studies have found that a LJ potential provides similar results qualitatively.[19] The dipole is approximated as a point dipole at the center of the particle consistent with previous calculations for the field created by a spherical magnetic particle.[19] This term has the same basic form for both magnetic and electric dipoles. Considering a magnetic dipole, the coefficients of the fit enabled a calculation of the net magnetic dipole moment, which ranged from $1\mathrm{e}^{-20}$ to $3\mathrm{e}^{-20}$ A·m^2 for particles with diameters 3 to 4 nm (Figure S13). The dipole moment increased with increasing particle volume as expected. We also estimated the magnetic dipole moment based on the known per formula unit magnetic dipole moment of the bulk material, which gave the same order of magnitude as our experimentally obtained value. This agreement further supported that it is the magnetic forces that are active in this experiment. Likewise, the magnitude of the van der Waals force, about twice thermal energy at the edge of the 1 nm ligand shell, is similar to previous theoretical estimates for magnetic particles and the fitted coefficients correlate to a reasonable Hamaker constant of about 10^{-19} J.[45,46]

These values not only demonstrate an approach to experimentally calculating fundamental nonbulk properties, but also help to explain and predict assembly behavior based on energy changes. When particles are initially randomly dispersed, the long-range dipole force acts to form chains. The net effect of multiple aligned dipoles in the chain favors further chain growth. However, because the dipolar force is on the order of thermal energy, the particles are not locked in chains (Figure 4d). Fluctuations of the location of the chained particles allow them to reconfigure to assume an even lower energy loosely packed arrangement, which maximizes neighbor contacts.

In order to quantify the energetic dynamics and stability of our assembly, we use our proposed nanoparticle interaction to calculate the change in energy from the observed configurations. A physically reasonable choice of a potential function representing forces will see total energy diminish over time. We calculate the total energy of a configuration by summing the interaction of each nanoparticle with all others

$$E_{\text{total}} = 0.5 \sum_{j}^{N} \sum_{i}^{N-1} U(l_{ij}, R_i, R_j, \hat{m}_i, \hat{m}_j)$$

Here $U(l, R, m)$ represents our interaction potential. Because the orientation of the particle dipoles is unknown, we estimate them using the lowest energy configuration. We consider each particle as fixed-point dipoles and let them "rotate freely" to find the lowest energy orientation (in practice, a minimization algorithm is used to minimize the overall energy with each variable being a dipole orientation). This approach led to realistic orientations; particles in chains and clusters had well-aligned dipoles (Figure 5a). This analysis demonstrated the loosely packed configuration had a lower average energy per particle compared to chains due to the favorable effect of the many nearby, aligned dipoles and close-range interactions (Figure 5b).

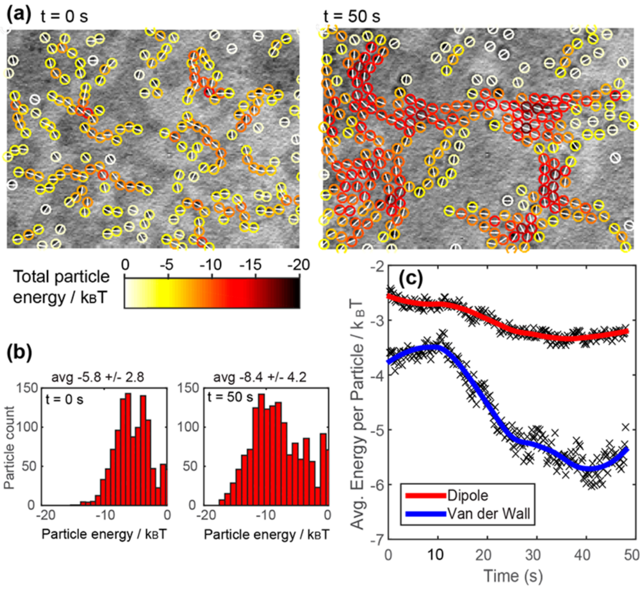

Figure 5. Energy and stability of self-assembly. (a) Colored circles indicate location of nanoparticles overlaid on original image. White arrows indicate dipole orientations. The color corresponds to the total energy of an individual nanoparticle computed from the dipole and van der Waal interaction with nearby particles. (b) The distribution of particle energies at two different time points. (c) The change in average particle energy contributions over time.

To disentangle the contributions from the different types of forces, the average particle dipole energy and the average van der Waal energy are tracked over time (Figure 5c). This indicated that although the dipole energy decreased over time, this was small compared to the large decrease in energy from close-range interactions. This demonstrates that the increase in neighbor contacts fundamentally drives the transition from chains to a packed lattice.

We note that electron beam interaction with the nanoparticles has been previously reported.[47,48] Under a highly focused electron beam (10^8A/m^2) with a high electron density gradient at the cross section, forces induced by electron beam field effects can be significant.[47] In this work, by maintaining a uniform electron density within the observed area and a low current density (10^5A/m^2) during the experiment, forces induced by the macroscopic electron beam field can be minimized. Along these lines, we also performed control experiments by growing pure platinum nanoparticles under identical observation conditions to that of the iron platinum particles (MovieS3). We found that the particles displayed no long-range attractions over a similar time scale. The results strongly support that the long-range forces and particle interactions observed for $PtFe_3$ were inherent particle magnetic properties and not merely an effect of the electron beam.

In summary, we have observed the complex dynamics of nanoparticle self-assembly directly, offering unprecedentedly quantitative insight into the mechanisms that underlie it. Using $PtFe_3$ particles, long-range anisotropic magnetic forces form chains in the initial stage of assembly, followed by chain folding to form loosely packed clumps that maximize close-range van der Waal interactions. Without a long-range electric or magnetic force, assembly might be driven merely by diffusion, taking significantly longer for nearby particles to associate permanently. The subtle interplay of close and long-range forces as well as the hierarchical process largely confirms the theories of earlier purely computational studies.

The direct observation of nanoparticle interaction to calculate the potential energy of interaction is an entirely new approach to understanding nonbulk fundamental properties. It also provides a means to quantitatively estimate the energetic stability of the observed assembly or any desired configuration of particles. This approach might easily be extended to many different materials using similar experiments and analyses. This detailed energetics information would significantly facilitate the accurate simulation of nanoparticle assembly in many different environments applicable to device fabrication.

■ ASSOCIATED CONTENT

Ⓢ Supporting Information

The Supporting Information is available free of charge on the ACS Publications website at DOI: 10.1021/acs.nanolett.6b02972.

Image analysis and particle tracking method description, configuration analysis description, additional assembly images, size distribution analysis, assembly spacing analysis, diffusion coefficient measurement, calculation of magnetic moment, calculation of interaction potential (PDF)

Rapid growth and assembly of PtFe nanoparticles at a resolution of 0.9 nm/pixel (AVI)

Rapid growth and assembly of PtFe nanoparticles at a resolution of 0.2 nm/pixel (AVI)

Pure platinum nanoparticles grown and imaged under identical conditions as Movie1 and Movie2 (MOV)

■ AUTHOR INFORMATION

Corresponding Author

*E-mail: hmzheng@lbl.gov.

Author Contributions

A.S.P. wrote the manuscript, developed all software code, performed data analysis, and initiated the project. H.G.L. performed all liquid cell experiments and imaging experiments. S.N.R. and N.D.B. contributed helpful discussion, background research, and theoretical analysis of nanoparticle properties. A.P.A. and H.Z. provided guidance. All authors edited the manuscript.

Notes

The authors declare no competing financial interest.

■ ACKNOWLEDGMENTS

We acknowledge the facility support from Molecular Foundry of Lawrence Berkeley National Laboratory (LBNL), which is supported by the U.S. Department of Energy Office of Basic Energy Sciences under Contract DE-AC02-05CH11231. H.Z. thanks the funding support from DOE Basic Energy Sciences Materials Sciences and Engineering Division.

■ REFERENCES

(1) Xie, Z.; Ellis, S.; Xu, W.; Dye, D.; Zhao, J.; Wang, Y. *Chem. Commun.* **2015**, *51* (81), 15000−3.

(2) Lee, S. H.; Yu, S. H.; Lee, J. E.; Jin, A.; Lee, D. J.; Lee, N.; Jo, H.; Shin, K.; Ahn, T. Y.; Kim, Y. W.; Choe, H. *Nano Lett.* **2013**, *13* (9), 4249−4256.

(3) Tan, H.; Santbergen, R.; Smets, A. H.; Zeman, M. *Nano Lett.* **2012**, *12* (8), 4070−6.

(4) Kamat, P. V. *J. Phys. Chem. C* **2008**, *112* (48), 18737−53.

(5) Granot, E.; Patolsky, F.; Willner, I. *J. Phys. Chem. B* **2004**, *108*, 5875−5881.

(6) Dai, Q.; Frommer, J.; Berman, D.; Virwani, K.; Davis, B.; Cheng, J. Y.; Nelson, A. *Langmuir* **2013**, *29* (24), 7472−7.

(7) Mohtasebzadeh, A. R.; Ye, L. *Int. J. Mol. Sci.* **2015**, *16* (8), 19769−19779.

(8) Dhar, J.; Patil, S. *ACS Appl. Mater. Interfaces* **2012**, *4*, 1803−1812.

(9) Zhong, C. J.; Maye, M. M. *Adv. Mater.* **2001**, *13* (19), 1507−11.

(10) Mendes, P. M.; Jacke, S.; Critchley, K.; Plaza, J.; Chen, Y.; Nikitin, K.; Palmer, R. E.; Preece, J. A.; Evans, S. D.; Fitzmaurice, D. *Langmuir* **2004**, *20* (9), 3766−8.

(11) Rao, S. G.; Huang, L.; Setyawan, W.; Hong, S. *Nature* **2003**, *425* (6953), 36−7.

(12) Talapin, D. V.; Lee, J. S.; Kovalenko, M. V.; Shevchenko, E. V. *Chem. Rev.* **2010**, *110* (1), 389−458.

(13) Baschek, J. E.; Klein, H. C.; Schwarz, U. S. *BMC Biophys.* **2012**, *5* (1), 22.

(14) Dobson, C. M. *Nature* **2003**, *426* (6968), 884−90.

(15) Whitesides, G. M.; Grzybowski, B. *Science* **2002**, *295* (5564), 2418−21.

(16) Knowles, T. W. *Nat. Nanotechnol.* **2010**, *5* (3), 204−207.

(17) Whitelam, S.; Feng, E. H.; Hagan, M. F.; Geissler, P. L. *Soft Matter* **2009**, *5* (6), 1251−62.

(18) Wilber, A. W.; Doye, J. P.; Louis, A. A.; Noya, E. G.; Miller, M. A.; Wong, P. *J. Chem. Phys.* **2007**, *127* (8), 085106.

(19) Ku, J.; Aruguete, D. M.; Alivisatos, A. P.; Geissler, P. L. *J. Am. Chem. Soc.* **2011**, *133*, 838−848.

(20) Sinyagin, A. Y.; Belov, A.; Tang, Z.; Kotov, N. A. *J. Phys. Chem. B* **2006**, *110* (14), 7500−7.

(21) Zhang, Z.; Tang, Z.; Kotov, N. A.; Glotzer, S. C. *Nano Lett.* **2007**, *7* (6), 1670−5.

(22) Rabani, E.; Reichman, D. R.; Geissler, P. L.; Brus, L. E. *Nature* **2003**, *426* (6964), 271−4.

(23) Min, Y.; Akbulut, M.; Kristiansen, K.; Golan, Y.; Israelachvili, J. *Nat. Mater.* **2008**, *7* (7), 527−38.

(24) Woehl, T. J.; Prozorov, T. *J. Phys. Chem. C* **2015**, *119*, 21261−21269.

(25) Tang, Z.; Kotov, N. A. *Adv. Mater.* **2005**, *17* (8), 951−62.

(26) Wu, L.; Shi, C.; Tian, L.; Zhu, J. *J. Phys. Chem. C* **2008**, *112* (2), 319−23.

(27) Lin, S.; Li, M.; Dujardin, E.; Girard, C.; Mann, S. *Adv. Mater.* **2005**, *17* (21), 2553−9.

(28) Hong, M.; Wu, L.; Tian, L.; Zhu, J. *Chem. - Eur. J.* **2009**, *15* (24), 5935−41.

(29) Cheng, G.; Romero, D.; Fraser, G. T.; Hight; Walker, A. R. *Langmuir* **2005**, *21* (26), 12055−9.

(30) Cho, K. S.; Talapin, D. V.; Gaschler, W.; Murray, C. B. *J. Am. Chem. Soc.* **2005**, *127* (19), 7140−7147.

(31) Talapin, D. V.; Shevchenko, E. V.; Murray, C. B.; Titov, A. V.; Král, P. *Nano Lett.* **2007**, *7*, 1213−1219.

(32) Shanbhag, S.; Kotov, N. A. *J. Phys. Chem. B* **2006**, *110* (25), 12211−7.

(33) Sánchez-Iglesias, A.; Grzelczak, M.; Altantzis, T. *ACS Nano* **2012**, *6* (12), 11059−11065.

(34) Margeat, O.; Tran, M.; Spasova, M.; Farle, M. *Phys. Rev. B: Condens. Matter Mater. Phys.* **2007**, *75*, 134410.

(35) Varón, M.; Pena, L.; Balcells, L.; Skumryev, V.; Martinez, B.; Puntes, V. *Langmuir* **2010**, *26* (1), 109−16.

(36) Zheng, H.; Smith, R. K.; Jun, Y. W.; Kisielowski, C.; Dahmen, U.; Alivisatos, A. P. *Science* **2009**, *324*, 1309−1312.

(37) Liao, H.; Cui, L. *Science* **2012**, *336*, 1011−1014.

(38) de Jonge, N.; Ross, F. M. *Nat. Nanotechnol.* **2011**, *6*, 695.

(39) Liu, Y. Z.; Lin, X. M.; Sun, Y. G.; Rajh, T. *J. Am. Chem. Soc.* **2013**, *135*, 3764−3767.

(40) Chadwick, G. A. *Met. Sci. J.* **1967**, *1* (1), 132−9.

(41) Cahn, J. W. *Acta Metall.* **1960**, *8* (8), 554−62.

(42) Kremser, G.; Rath, T.; Kunert, B.; Edler, M.; Fritz-Popovski, G.; Resel, R.; Trimmel, G. *J. Colloid Interface Sci.* **2012**, *369* (1), 154−159.

(43) Chen, M. *Langmuir* **2007**, *23* (10), 5296−5304.

(44) de la Presa, P. *IEEE Trans. Magn.* **2008**, *44* (11), 2816−2819.

(45) Lalatonne, Y.; Richardi, J.; Pileni, M. P. *Nat. Mater.* **2004**, *3*, 121−125.

(46) Hamaker, H. C. *Physica* **1937**, *4*, 1058−1072.

(47) Zheng, H. *Nano Lett.* **2012**, *12* (11), 5644−5648.

(48) Batson, P. E. *Nano Lett.* **2011**, *11* (8), 3388−3393.